FRONTIERS OF PHYSICS

RESEARCH ARTICLE
Volume 18 / Issue 4 / 42300 / 2023

Characteristics investigation of Yb^{3+}:YAG crystals for optical refrigeration

Yongqing Lei[1,2], Biao Zhong[1,†], Xuelu Duan[1], Chaoyu Wang[1], Jiajin Xu[1], Ziheng Zhang[1], Jinxin Ding[1], Jianping Yin[1,‡]

1 State Key Laboratory of Precision Spectroscopy, East China Normal University, Shanghai 200062, China
2 Shanxi Vocational University of Engineering Science and Technology, Jinzhong 030619, China
Corresponding authors. E-mail: †bzhong@lps.ecnu.edu.cn, ‡jpyin@phy.ecnu.edu.cn
Received July 27, 2022; accepted November 3, 2022

ABSTRACT

Yb^{3+}:YAG crystal is one excellent material for developing high-power radiation-balanced lasers (RBLs). An experimental study of the laser cooling performances of YAG crystals with various doping Yb^{3+} concentrations, especially for application of RBLs, is reported here. With improved Yb^{3+} doping concentration in YAG crystal, though the resonance absorption coefficient increases, the corresponding external quantum efficiency has been found to decrease with the average fluorescence wavelength being red shifted, which is detrimental to anti-Stokes fluorescence (ASF) cooling. The decrease of the external quantum efficiency can cause the first zero crossing wavelength to red shift, which is not conducive to RBLs. Based on the comprehensive study of the cooling characteristics of the series of Yb^{3+}-doped YAG crystals, the optimal Yb^{3+} doping concentration for ASF cooling has been suggested.

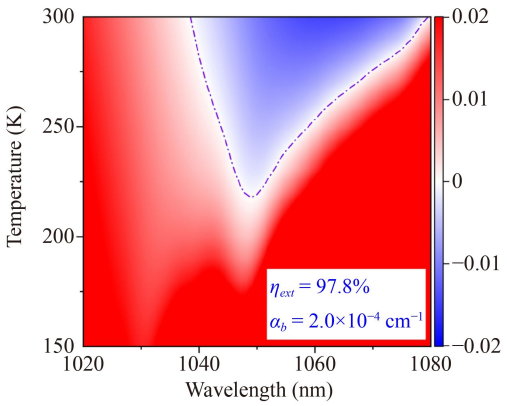

Keywords anti-Stokes fluorescence cooling, Yb^{3+}:YAG crystal, radiation-balanced lasers

1 Introduction

Laser cooling is the physical processes in which materials interact with laser and lose kinetic or thermal energy, where the materials can be gases [1–4], liquids [5], and solids [6–8]. Compared with laser cooling in gases, the reduced thermal energy of which is mainly from translational degrees of freedom, the reduced thermal energy in laser-cooled solids is from lattice vibrations [9]. Laser cooling of gases involves the cooling and trapping of atoms and molecules, which is now a workhorse in many fields, including quantum computer, quantum information, time/frequency standards and tests of fundamental physics [10–19]. Laser cooling of solids recently has received great attention benefit from important applications in airborne and space-based sensor systems, optical tweezers and precision metrology [20–24].

The net laser cooling of Yb^{3+}:ZBLANP glasses by Epstein *et al.* in 1995 [6] confirmed the earlier idea of ASF cooling of bulk matter proposed by Pringsheim [25] and thermodynamic analysis of ASF cooling given by Landau [26]. Since then, ASF cooling has been confirmed in of sorts glasses and crystals doped with trivalent rare-earth ions, such as Yb^{3+}, Tm^{3+}, and Ho^{3+}[6, 7, 27–29]. In particular, Yb^{3+}:YLF [7, 8, 30, 31] and Yb^{3+}:LLF [32–34] have achieved remarkable cooling temperature records which are below the cryogenic temperature 123 K. ASF cooling of semiconductors has also attracted great attention of researchers. Big advances have made in both theory and experiment [35–37]. In theory, the Fermi-Dirac distribution governed charge carriers enable semiconductors to be

https://doi.org/10.1007/s11467-023-1266-6

laser cooled even colder than the rare-earth-doped materials, however experimental studies are still at an early stage [9, 35, 36, 38–40].

Shortly after demonstration the idea of ASF cooling in experiment, the concept of RBLs was introduced by Bowman in 1999 [41]. The ASF cooling is used to remove the heat load coming from both the quantum defect and the parasitic absorption of the impurities in laser operation [42–44]. Laser operation with no net heat generation in the gain medium is desirable not only for high power laser output, but also for applications in low-noise sensing and high precision metrology [45–47].

One of the big challenges in stable operation of the RBLs and radiation-balance amplifiers (RBAs) is to keep a very subtle balance condition between different cooling and lasing parameters [47–49]. Following the advancement in theory of RBLs and RBAs, experimental progress has been greatly achieved in recent years [23, 47, 50–57]. Recently, RBLs based on fibers of silica and ZBLAN with extremely low OH^- and suppressed Yb^{3+} ion clustering have also been experimentally demonstrated [23, 49]. Yb^{3+}:YAG as one of the excellent laser gain media, featuring high thermal conductivity, low electron-phonon coupling rates and well-developed annealing technology, has also good laser cooling performance. In 2001, Epstein *et al.* [58] pumped 2.3% Yb^{3+}:YAG crystal at 1030 nm in a vacuum and obtained a temperature drop of 8.9 K from room temperature. In 2013, de Lima Filho *et al.* [59] pumped 3% Yb^{3+}:YAG crystal at 1030 nm in atmosphere and achieved a temperature drop of 8.8 K from room temperature [59]. Recently, our group obtained a temperature drop of about 80 K in the 3% Yb^{3+}:YAG crystal by laser at 1030 nm in vacuum [60]. In addition, the Yb^{3+}:YAG crystals of both rod and disk geometry have also been experimentally demonstrated as the gain medium for RBLs [42, 53].

Yb^{3+}:YAG crystal is generally considered as a promising gain medium for RBLs, whose performance depends on the cooling behavior of the crystal [42, 53]. The Yb^{3+} doping concentration strongly affects the crystal in its cooling behavior [55]. In theory, higher dopant concentration will benefit the laser output power since more Yb^{3+} ions are involved in the lasing and cooling cycles, however other factors like concentration quenching will also get serious and thus affect the laser performance. Therefore, a comprehensive research about the relationship between the ASF cooling characteristics of the crystal and the dopant concentration is necessary. In this paper, we experimentally investigate the laser cooling performance of YAG crystals with various doping Yb^{3+} concentrations. The Yb^{3+} doping concentration dependent laser cooling characteristics of the samples are analyzed in detail. And the optimum doping Yb^{3+} concentration for ASF cooling is suggested.

The principle of laser cooling of rare-earth doped solids is based on ASF processes [25]. Rare-earth ions are excited by photons of energy $h\nu_p$ from the top of the ground state to the bottom of the excited state. The excited ions reach quasi-equilibrium with the lattices of the host by absorbing phonons. Then the excited ions spontaneously radiatively decay to the ground state emitting the anti-Stokes fluorescence photons of mean photon energy $h\nu_f$, which are higher than the absorbed photons in energy. The energy difference between $h\nu_f$ and $h\nu_p$ is supplied by the host and taken away by ASF. The four-level theoretical model is conventionally used to characterize the cooling efficiency and expressed as [61]

$$\eta_c = \eta_{ext}\eta_{abs}\frac{\lambda_p}{\lambda_f} - 1, \tag{1}$$

where λ_p and λ_f are the pump and mean fluorescence wavelength, respectively. $\eta_{ext} = \eta_e W_r/(\eta_e W_r + W_{nr})$ and $\eta_{abs} = \alpha_r/(\alpha_r + \alpha_b)$ represent the external quantum efficiency and absorption efficiency, respectively. η_e is the fluorescence extraction efficiency related to the reabsorption and the total internal reflection (TIR) in the host. W_r and W_{nr} are the radiation and non-radiation decay rate, respectively. The α_r and α_b are the resonant and background absorption coefficient, respectively.

The mean fluorescence wavelength λ_f of the Yb^{3+}:YAG crystal can be calculated according to the following expression [62]:

$$\lambda_f^{theo} = \frac{c}{\nu_f} = \frac{c\left(\sum_j^3\sum_i^4 f_{1j}\beta_{0i}^{1j}\right)}{\sum_j^3\sum_i^4 f_{1j}\beta_{0i}^{1j}\nu_{0i}^{1j}}, \tag{2}$$

where the superscript theo in λ_f^{theo} is short for theoretical. $f_{0i}\,(i = 1, 2, 3, 4)$ and $f_{1j}\,(j = 1, 2, 3)$ are the Boltzmann occupation factors of the Stark sublevels of the ground and excited states of Yb^{3+} ion, respectively. The expressions of f_{0i} and f_{1j} are described as follows:

$$f_{0i} = \frac{\exp\left(-\frac{E_{0i}}{k_B T}\right)}{\sum_i^4 \exp\left(-\frac{E_{0i}}{k_B T}\right)}, \tag{3a}$$

$$f_{1j} = \frac{\exp\left(-\frac{E_{1j}}{k_B T}\right)}{\sum_j^3 \exp\left(-\frac{E_{1j}}{k_B T}\right)}, \tag{3b}$$

where, k_B is the Boltzmann constant, E_{0i} and E_{1j} represent the energy of the sublevels in the ground state ($^2F_{7/2}$) and excited state ($^2F_{5/2}$), respectively. β_{0i}^{1j} is the branching ratio of the Yb^{3+}:YAG crystal. ν_{0i}^{1j} is the transition frequency between the energy levels from the excited state sublevel (1, j) to the ground state sublevel (0, i).

2 Experimental setup

Figure 1 shows the schematic of the experimental setup

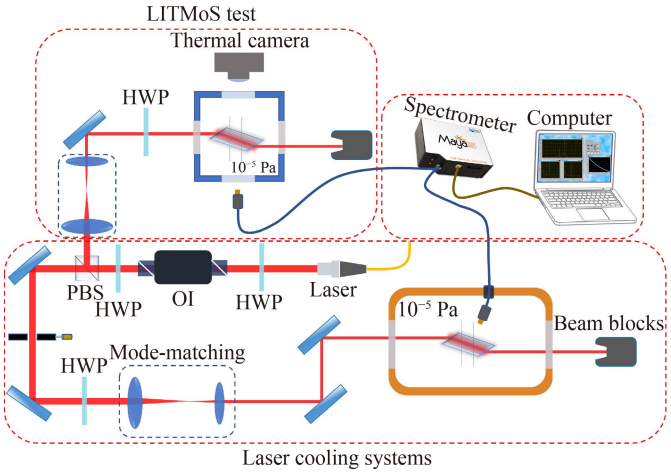

Fig. 1 The schematic diagram of the LITMoS test and laser cooling experimental setup. HWP: half-wave plate; OI: optical isolator; PBS: polarizing beam splitter.

including the LITMoS (Laser Induced Temperature Modulation Spectrum) test system and laser cooling system. A fiber laser (YFL-1020-50, Precilasers Co. Ltd.) with a tunable wavelength range of 1010–1080 nm is used for both the LITMoS test and laser cooling experiments. An optical isolator prevents unwanted light feedback into the laser system. The combination of a half-wave plate (HWP) and a polarization beam splitter (PBS) divides the linearly polarized laser into two branch beams with adjustable power for LITMoS test and laser cooling experiments.

The laser cooling characteristics of the sample, η_{ext} and α_b are obtained by fitting the cooling efficiency $\eta_c^{\exp}(\lambda) = K \cdot \Delta T / P_{abs}$ measured by the LITMoS test using Eq. (1) [63, 64]. The laser irradiates the sample with its wavelength varying from 1010 nm to 1080 nm at an interval of 10 nm to produce the small temperature change ΔT (heating or cooling). The spectrometer and the calibrated thermal camera are used to measure the absorption power P_{abs} and ΔT, respectively. K is a constant related to the thermal load on the sample. It is essential that the ambient temperature is kept stable and thermal equilibrium is achieved in the sample for each measurement. A pair of mode-matching lenses is used to adjust the waist radius of the laser beam incident onto the Yb^{3+}:YAG crystal of dimension $2\times2\times5$ mm^3 at Brewster angle cut. A multimode fiber with diameter 600 μm collects the fluorescence light emitted by the crystal and transfers it to the spectrometer. The sample is placed in a vacuum chamber (10^{-5} Pa) and supported by two optical fibers (diameter 100 μm), blackbody radiation of the vacuum chamber is the primary source of heat load.

The optical probe system is calibrated by a standard blackbody radiation source (Ocean Optics HL-3P-INT-CAL-EXT). A calibrated thermal camera is adopted to measure the laser-induced temperature changes of the sample during the LITMoS test, while differential luminescence thermometry [7] is adopted to measure the temperature of the sample in the laser cooling experiment. The temperatures of the crystal and the environment are monitored in real-time.

3 Cooling efficiency parameters

3.1 Absorption efficiency and the mean fluorescence wavelength with different Yb^{3+} doping concentration

Figure 2(a) shows the Stark sublevel energies of Yb^{3+}:YAG crystal at room temperature [65] and the cooling cycle of optical refrigeration. The red upward arrow indicates the pump laser with wavelength λ_p, and the blue downward arrow indicates the fluorescence with a mean wavelength of λ_f. The blue and red solid lines in figure 2(b) represent the absorption and the fluorescence

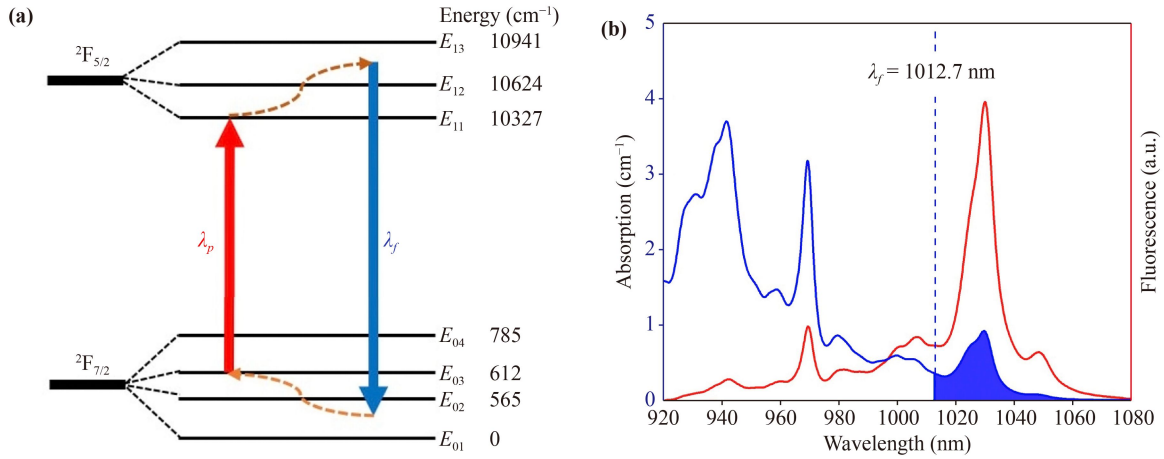

Fig. 2 **(a)** The energy diagram of the Yb^{3+} in YAG crystal. **(b)** Absorption (blue) and fluorescence (red) spectra for the 5% Yb^{3+}:YAG crystal at 300 K. The blue dotted line indicates the mean fluorescence wavelength λ_f at 300 K.

spectra of the 5% Yb^{3+}:YAG crystal, respectively. The blue dash-dot line represents λ_f of the 5% Yb^{3+}:YAG crystal at 300 K, appearing at about 1012.7 nm. The blue shaded region to the right of λ_f under the absorption spectrum is called the "optical cooling tail." The pump wavelength for laser cooling should be chosen inside the optical cooling tail. Since the resonance absorption coefficient is small in the blue shaded region, the utilization of the pump power is low in efficiency.

Temperature-dependent fluorescence spectra of the sample, placed in the cold finger in a high vacuum liquid nitrogen cryostat (JANIS VPF-100) for adjusting the temperature, were excited by the laser at 914 nm with the power less than 3 mW, and were measured by a calibrated spectrometer (Ocean Optics Maya2000 Pro-NIR) through a multimode fiber with the diameter of 600 μm. Figure 3(a) shows the temperature-dependent fluorescence spectra of the 5% Yb^{3+}:YAG crystal from 150 K to 300 K at an interval of 50 K. The resonant absorption coefficient $\alpha_r(\lambda, T)$ is obtained from the fluorescence spectrum $S(\lambda, T)$ utilizing the McCumber relation $\alpha_r(\lambda, T) \propto \lambda^5 S(\lambda, T) \exp\left(\frac{hc}{\lambda k_B T}\right)$ [66] combined with the normalization at the wavelength of 1030 nm, and corresponding results are shown in Fig. 3(b). As one can see, in the optical cooling tail there are two peaks located at 1030 nm and 1048 nm, respectively. The absorption coefficient in the optical cooling tail rapidly decreases as the sample temperature is reduced.

The λ_f of the Yb^{3+}:YAG crystal can be obtained from

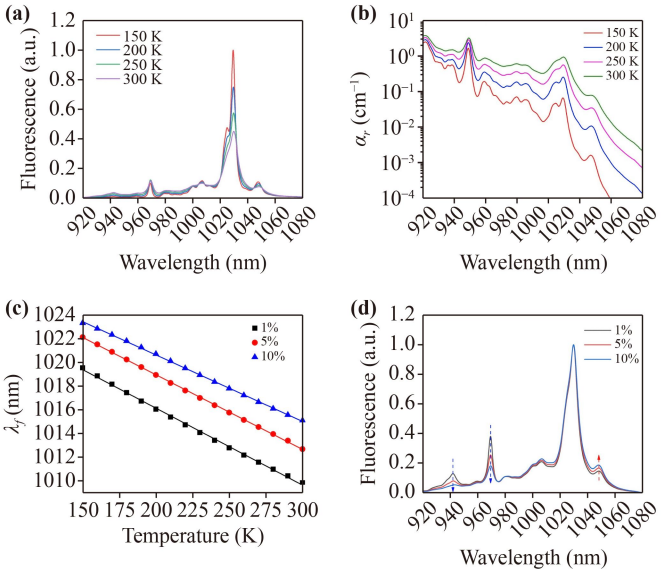

Fig. 3 The temperature-dependent fluorescence **(a)** and absorption **(b)** spectra for the 5% Yb^{3+}:YAG crystal, respectively. **(c)** The mean fluorescence wavelength λ_f for 1%, 5% and 10% Yb^{3+}:YAG versus the temperature of the sample. The solid line indicates a linear fitting. **(d)** The normalized fluorescence spectrum for 1%, 5% and 10% Yb^{3+}:YAG at 300 K.

the measured fluorescence spectrum by utilizing the following formula [63]:

$$\lambda_f^{exp}(T) = \frac{\int S(\lambda, T)\,\lambda \mathrm{d}\lambda}{\int S(\lambda, T)\,\mathrm{d}\lambda}, \tag{4}$$

where the superscript exp in λ_f^{exp} is short for experimental. $S(\lambda, T)$ is the temperature-dependent fluorescence spectra of the sample. Figure 3(c) shows the dependence of λ_f on the sample temperature. The solid black squares, red circles, and blue triangles represent results for selected Yb^{3+} doping concentrations of 1%, 5%, and 10%, respectively. All measurements are fitted by linear functions and given as follows: $\lambda_f^{1\%} = -0.065$ (nm/K) × T (K) + 1029.14 (nm), $\lambda_f^{5\%} = -0.063$ (nm/K) × T (K) + 1031.56 (nm), and $\lambda_f^{10\%} = -0.056$ (nm/K) × T (K) + 1031.87 (nm). The value of λ_f gets red shifted with the decrease of the sample temperature, which causes more populations on the lower sublevels of the excited state governed by Boltzmann statistics.

Eq. (2) is used to calculate the dependence of the mean wavelength λ_f on the sample temperature. For instance, the theoretically calculated values are λ_f (300 K, 1%) = 1009.2 nm and λ_f (80 K, 1%) = 1011.6 nm, respectively. The experimentally measured values are λ_f (300 K, 1%) = 1009.6 nm and λ_f (80 K, 1%) = 1024.2 nm, respectively. As one can see, the difference at high temperature between theoretical calculation and experimental measurement is rather small, while that at low temperature is quite large. The large discrepancy at low temperature mainly comes from that the temperature dependence of the branching ratio is not considered in Eq. (2). Besides, the cooperative effect and reabsorption related to Yb^{3+} ion concentration and crystal shape also affect the value of λ_f. For example, at a fixed temperature of 300 K, the value of λ_f from experimental measurement is redshifted by about 5.3 nm when the Yb^{3+} doping concentration increases from 1% to 10%, as can be seen in Fig. 3(c). This red shift is ascribed to the effect of fluorescence reabsorption. Fluorescence reabsorption and trapping tend to be more effective as the Yb^{3+} doping concentration increases, resulting in more depleted emissions at higher energies [67]. Figure 3(d) shows the fluorescence spectra of 1%, 5%, and 10% Yb^{3+}:YAG crystals at 300 K. All the curves are normalized at wavelength 1030 nm for better comparison. As one can see, with increasing Yb^{3+} doping concentration, the intensity of the fluorescence at wavelength shorter than 980 nm gets weaker, while that at wavelength longer than 980 nm gets stronger.

3.2 External quantum efficacy and with different Yb^{3+} doping concentration

The external quantum efficiency η_{ext} and the background absorption coefficient α_b of the 1%, 5%, and 10% Yb^{3+}:

YAG crystal samples are measured by the LITMoS test. Figure 4 shows the corresponding results with the solid circles representing the experimental data of cooling efficiency at 300 K. The values of η_{ext}, α_b and the cooling range (300 K) between two zero-crossing wavelengths (λ_{c1}–λ_{c2}) are obtained by the model fit utilizing Eq. (1) and were listed in Table 1. The variation of the background absorption α_b among different samples is small. With increasing Yb^{3+} doping concentration, the second zero-crossing wavelength λ_{c2} is red shifted, which is attributed to the increasing absorption efficiency $\eta_{abs} = 1/(1 + \alpha_b/\alpha_r)$.

As shown in Table 1, the value of η_{ext} decreases with increasing the Yb^{3+} doping concentrations, which is consistent with the theoretical prediction in Ref. [68]. Besides, a higher Yb^{3+} doping concentration will lead to a relatively larger refractive index of the sample [69], resulting in more fluorescence confinement and reabsorption, migration of excited electrons, and cooperative luminescence [68]. A well-known formula generalizes the influence of cooperative effects on the fluorescence lifetime τ_f of excited energy levels, and given as [70]

$$\tau_f = \frac{\tau_w\,(1+\sigma N_{\mathrm{Yb}} l)}{1+\frac{9}{2\pi}\left(\frac{N_{\mathrm{Yb}}}{N_0}\right)^2}, \tag{5}$$

where $\tau_w = 0.95$ ms is the measured lifetime at low concentration [71], σ is the absorption cross-section, l is the average absorption length, N_{Yb} is the number density of doped Yb^{3+} ions, and $N_0 = 2.3 \times 10^{21}$ cm^{-3} is a critical Yb^{3+} ion density (corresponding to doping concentration of ~17%) for concentration quenching [71]. It is necessary to control the Yb^{3+} doping concentration in YAG crystals so that the corresponding number density is much lower than N_0 to avoid concentration quenching. The fluorescence lifetime τ_f can also be described as $\tau_f = \eta_e/(\eta_e W_r + W_{nr})$, $W_{nr} = W_{mp} + \Sigma_i W_i$ [50]. Here, W_{mp} ~2.12×10^{-6} s^{-1} is the multiphonon non-radiative decay rate at 300 K [72] and $\Sigma_i W_i$ is the sum of non-radiative decay rates of other channels from the sublevel related. The condition of $W_{nr} \ll W_r$ is necessary in order to obtain a high external quantum efficiency η_{ext}. When N_{Yb} is increased from 1% to 10%, τ_f is reduced by 18% due to increasing non-radiative decay rates according to Eq. (5), and this will result in significant decrease of η_{ext}. The decreasing η_{ext} can result in red shift of the first zero-crossing wavelength λ_{c1}.

On the basis of the laser cooling parameters of the Yb^{3+}:YAG crystal samples, the cooling efficiency contour diagram, named as "cooling window", of each sample are drawn utilizing the theoretical model expressed by Eq. (1). The cooling window can comprehensively describe the laser cooling feature of the sample. Figures 5(a–c) show the cooling windows of 1%, 5% and 10% Yb^{3+}:YAG crystals, respectively. The Yb^{3+}:YAG crystal has resonance absorption peaks at 1030 nm and 1048 nm in the optical cooling tail, corresponding to the $E_{03}\rightarrow E_{11}$ and $E_{04}\rightarrow E_{11}$ Stark sublevel transitions. When the Yb^{3+} doping concentration increases from 1% to 10%, the cooling range generally moves toward the longer wavelength and the optimal pump wavelength for cooling changes from 1030 nm to 1048 nm. The above comparative study indicates that the 5% Yb^{3+}:YAG crystal exhibits excellent cooling performance, with a

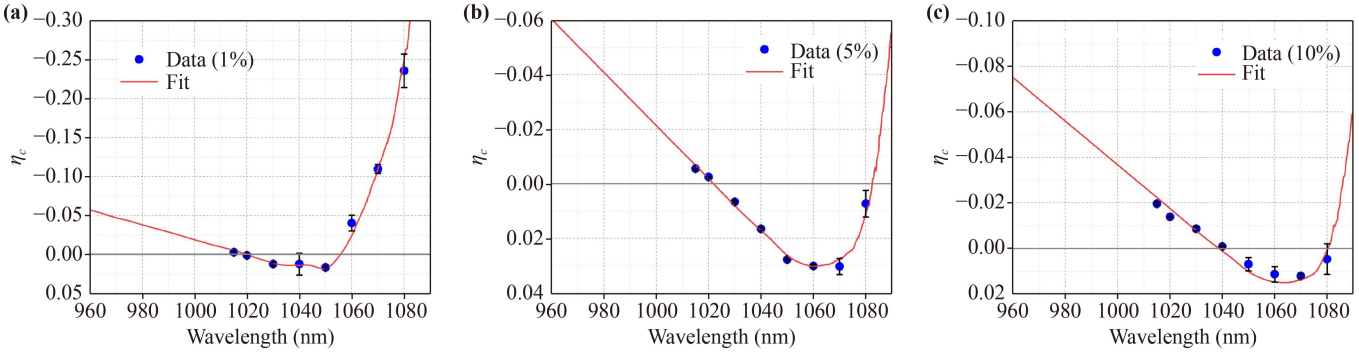

Fig. 4 Experimental results (blue solid circles) and model fitting (red lines) to cooling efficiency for the 1% **(a)**, 5% **(b)** and 10% **(c)** Yb^{3+}:YAG crystals at 300 K.

Table 1 The results of the LITMoS test.

Sample	Parameters		
	η_{ext}	α_b	Cooling range (λ_{c1}–λ_{c2})
1% Yb^{3+}:YAG	99.20%	1.6×10^{-4} cm^{-1}	1020–1055 nm
5% Yb^{3+}:YAG	99.15%	1.0×10^{-4} cm^{-1}	1022–1082 nm
10% Yb^{3+}:YAG	97.80%	2.0×10^{-4} cm^{-1}	1038–1080 nm

cooling window predicted global minimum achievable temperature (g-MAT) of about 180 K.

4 Laser cooling results

The cooling windows shown in Fig. 5 indicate that the optimum pump wavelength for the 1% and 5% Yb^{3+}:YAG crystals is 1030 nm, while that for the 10% Yb^{3+}:YAG crystal is 1048 nm. For simplicity, the single-pass configuration of pump laser is adopted to characterize the optical cooling properties of the YAG crystal samples with various Yb^{3+} doping concentrations. The crystal temperature reaches a steady state under the combined effect of laser cooling and black body radiation heating. The laser cooling power (P_{cool}) and the heat load power (P_{load}) are described by the following equations [73]:

$$P_{cool} = P_{pump}\left[1 - \exp\left(-\alpha_r l\right)\right]\eta_c, \tag{6a}$$

$$P_{load} = \varepsilon_s A_s \sigma\left(T_c^4 - T^4\right) + \frac{N\kappa_L A_L}{d_L}\left(T_c - T\right), \tag{6b}$$

where P_{pump} is the incident laser power, and l is the crystal's length. The Stefan–Boltzmann constant $\sigma = 5.67 \times 10^{-8}$ W/(m^2·K^4), T_c is the temperature of the vacuum chamber. ε_s and A_s represent the emissivity and the surface area of the sample, respectively. N is the number of contacting points with area A_L, length d_L and conductivity κ_L. Figure 6(a) describes the temperature of each sample varying with the pump laser power. The solid symbols correspond to experimental measurements with the solid line being the model fitted lines from Eqs. 6(a) and (b). In our experiment, with a pump power of about 35 W the finally obtained cooling temperatures are 252 K, 226 K and 261 K for the 1%, 5% and 10% Yb^{3+}:YAG crystals, respectively. The time-dependent temperature evolution of each sample is shown in Fig. 6(b). The temperature drops are 42 K, 69 K, and 34 K for the 1%, 5%, and 10% Yb^{3+}:YAG crystals, respectively. It usually takes about 10 minutes for the sample to reach the final equilibrium state in temperature.

5 Discussion and conclusions

The cooling efficiency η_c of the sample is determined by four parameters η_{ext}, α_r, λ_f and α_b. Three of them η_{ext}, α_r and λ_f are affected by the Yb^{3+} doping concentrations. Figures 7 (a) and (b) show the corresponding experimental results. When the doping concentration increases from 1% to 10%, the mean fluorescence wavelength λ_f is redshifted from 1009.2 nm to 1015.1 nm, and the external quantum efficiency η_{ext} decreases from 99.2% to 97.8%. When the Yb^{3+} doping concentration exceeds 5%, there is a dramatic drop in η_{ext}. This observation is greatly different from the theoretical calculation in Ref. [68], where η_{ext} decreases slowly and slightly with the Yb^{3+} doping concentration increasing up to 10%. Our explanation is as follows: as the Yb^{3+} doping concentration increases, more Yb^{3+} ions participate in the laser cooling cycle, and the resonance absorption of the pump laser increases, so do the fluorescence reabsorption and trapping effect. However, the enhanced fluorescence reabsorption and trapping effect result in a redshift of the λ_f and thus the decrease of η_{ext}. For the 7.5% and 10% Yb^{3+}:YAG crystals under our study here, this causes the first zero-crossing wavelength λ_{c1} to exceed 1030 nm. Therefore, for laser cooling of Yb^{3+}:YAG crystals with doping concentrations greater than 7.5%, the pump laser wavelength should be tuned to 1048 nm for optimum cooling effect.

Compared to the 2% and 7.5% Yb^{3+} doped samples, the 1%, 5% and 10% Yb^{3+} doped ones are superior and close in quality and have a smaller background absorption, and therefore their cooling performances are selectively picked out and presented in Fig. 6 for better comparison. Furthermore, for a better understanding of the influence of the dopant concentration on the ASF cooling behavior the background absorption coefficients of the six samples are compiled in Fig. 7(c) and their

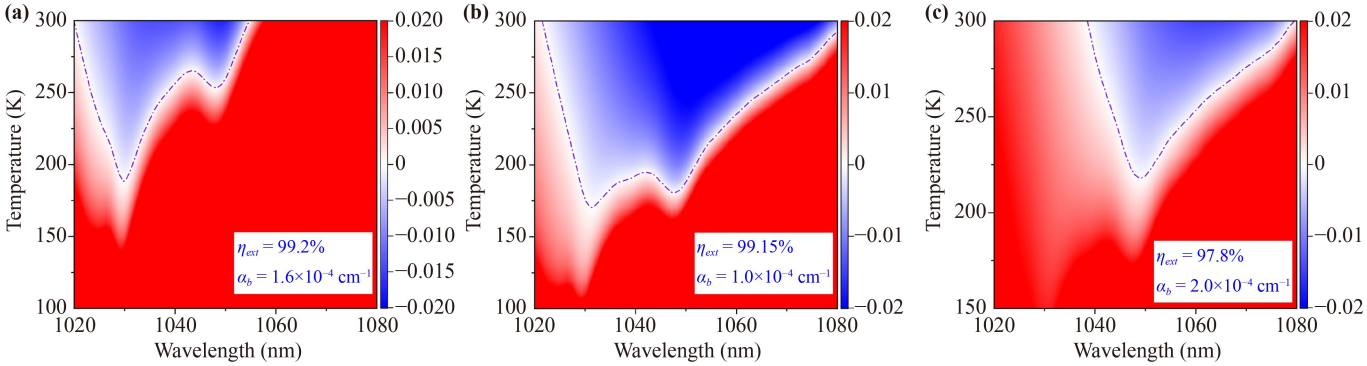

Fig. 5 The cooling windows of the 1% **(a)**, 5% **(b)** and 10% **(c)** Yb^{3+}:YAG crystals. The blue and red regions correspond to the cooling and heating regimes, respectively, with the dotted lines representing $\eta_c = 0$.

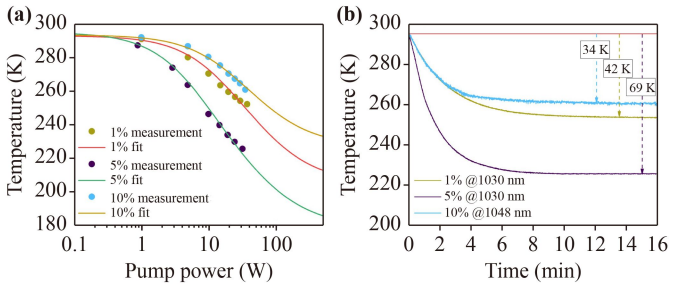

Fig. 6 **(a)** Steady-state temperature of the 1%, 5% and 10% Yb^{3+}:YAG crystals versus the power of pumping laser. Dots represent the measurement data and lines represent the model prediction. **(b)** Time-dependent evolution of the 1%, 5% and 10% Yb^{3+}:YAG crystals.

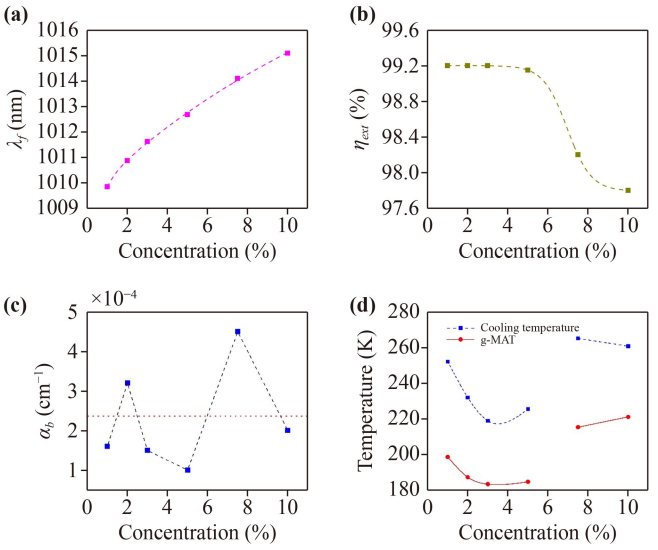

Fig. 7 **(a)** Concentration dependence of the mean fluorescence wavelength λ_f (300 K). **(b)** Concentration dependence of the external quantum efficiency η_{ext}. **(c)** The background absorption coefficients of each sample. The red line indicates the average value of the background absorption coefficient (2.3×10^{-4} cm^{-1}). **(d)** Concentration dependence of the minimum cooling temperature of each sample obtained in the experiment with the pump laser of about 35 W and the g-MAT of each sample with the same average background absorption coefficient (2.3×10^{-4} cm^{-1}).

average value $\alpha_b = 2.3 \times 10^{-4}$ cm^{-1} is calculated and shown by the dotted line. The final cooling temperature obtained in our experiment of each sample under the same experimental conditions including the pump power of about 35 W is presented in Fig. 7(d) in blue solid squares. Experimental results in Fig. 7(d) show that the final cooling temperature of the 7.5% Yb^{3+}:YAG crystal is slightly higher than the 10% Yb^{3+}:YAG crystal. This is ascribed to their slight difference of various samples in their impurity absorption and scattering. Experimental measurement indicates the background absorption is 4.5×10^{-4} cm^{-1} and 2×10^{-4} cm^{-1} for the 7.5% and 10% Yb^{3+}:YAG crystals, respectively. The g-MAT of the six samples are also calculated from their respective cooling parameters with the same average background absorption coefficient and corresponding results are shown in Fig. 7(d) in red circles. As we can see, the results follow the trend of those from experiment and indicates an optimal doping concentration in the range of 3%–5%.

In conclusion, the optical cooling characteristics of the YAG crystals with the Yb^{3+} doping concentrations ranging from 1% to 10% are comprehensively studied in experiment. The fluorescence spectra with the sample temperature range of 150–300 K are accurately measured and the corresponding absorption spectra are carefully obtained. The external quantum efficiency η_{ext} and the background absorption α_b are precisely measured by the LITMoS test. The influences of the Yb^{3+} doping concentration on the cooling parameters of λ_f, η_{ext} and α_r are analyzed. The cooling windows are also mapped to characterize the optical cooling properties of the samples. As the sample temperature decreases, the experimentally measured red shift of the mean fluorescence wavelength λ_f deviates more from its corresponding theoretical calculation. For instance, the deviation of λ_f for the 1% Yb^{3+}:YAG crystal at a temperature of 300 K is about 0.4 nm, while that at 80 K increases to about 12.6 nm. As the Yb^{3+} doping concentration increases, the experimentally measured external quantum efficiency η_{ext} decreases more dramatically compared to its corresponding slight change from theoretical calculation, particularly for samples with doping concentration larger than ~5%. For instance, the value of η_{ext} for the 1% Yb^{3+} and 10%:YAG crystal in our experiment is measured to be ~99.2% and ~97.6% respectively, corresponding to a variation of ~1.6%, while that from the theoretical calculation is less than ~0.2% [68]. This dopant concentration-dependent value of η_{ext} has a strong influence on the optical cooling behavior of the sample and thus the finally obtained temperature. As one can see, as the Yb^{3+} doping concentration improves, though the resonant absorption will be increased, the decreasing external quantum efficiency η_{ext} and the red shifting mean fluorescence wavelength λ_f will impair the total cooling efficiency. Our comprehensive studies suggest an optimal dopant concentration of about 3%–5% for the Yb^{3+}:YAG crystals of similar sizes for optical cooling performance. We believe the results presented here can serve as a helpful reference for researchers involved in related studies, like optical coolers and RBLs.

Acknowledgements This research was supported by the National Natural Science Foundation of China (Grant Nos. 11604100, 11834003, 61574056, 91536218, and 11874151), the Special Financial Grant from the China Postdoctoral Science Foundation (Grant No. 2016T90346), and 111 Project (No. B12024). B. Zhong thanks L. Z. Deng for helpful discussions.

References

1. N. Djeu and W. Whitney, Laser cooling by spontaneous anti-Stokes scattering, *Phys. Rev. Lett.* 46(4), 236 (1981)
2. E. A. Cornell and C. E. Wieman, Bose–Einstein condensation in a dilute gas, the first 70 years and some recent experiments, *Rev. Mod. Phys.* 74(3), 875 (2002)
3. T. W. Hänsch and A. L. Schawlow, Cooling of gases by laser radiation, *Opt. Commun.* 13(1), 68 (1975)
4. D. S. Jin and J. Ye, Polar molecules in the quantum regime, *Phys. Today* 64(5), 27 (2011)
5. C. Zander and K. H. Drexhage, Cooling of a dye solution by anti-Stokes fluorescence, *Adv. Photochem.* 20, 59 (1995)
6. R. I. Epstein, M. I. Buchwald, B. C. Edwards, T. R. Gosnell, and C. E. Mungan, Observation of laser-induced fluorescent cooling of a solid, *Nature* 377(6549), 500 (1995)
7. D. V. Seletskiy, S. D. Melgaard, S. Bigotta, A. Di Lieto, M. Tonelli, and M. Sheik-Bahae, Laser cooling of solids to cryogenic temperatures, *Nat. Photonics* 4(3), 161 (2010)
8. S. D. Melgaard, A. R. Albrecht, M. P. Hehlen, and M. Sheik-Bahae, Solid-state optical refrigeration to sub-100 Kelvin regime, *Sci. Rep.* 6(1), 20380 (2016)
9. D. V. Seletskiy, R. Epstein, and M. Sheik-Bahae, Laser cooling in solids: Advances and prospects, *Rep. Prog. Phys.* 79(9), 096401 (2016)
10. W. D. Phillips, Nobel Lecture: Laser cooling and trapping of neutral atoms, *Rev. Mod. Phys.* 70(3), 721 (1998)
11. I. Bloch, J. Dalibard, and W. Zwerger, Many-body physics with ultracold gases, *Rev. Mod. Phys.* 80(3), 885 (2008)
12. A. D. Ludlow, M. M. Boyd, J. Ye, E. Peik, and P. O. Schmidt, Optical atomic clocks, *Rev. Mod. Phys.* 87(2), 637 (2015)
13. R. Horchani, Laser cooling of internal degrees of freedom of molecules, *Front. Phys.* 11(4), 113301 (2016)
14. J. L. Bohn, A. M. Rey, and J. Ye, Cold molecules: Progress in quantum engineering of chemistry and quantum matter, *Science* 357(6355), 1002 (2017)
15. S. A. Malinovskaya, Laser cooling using adiabatic rapid passage, *Front. Phys.* 16(5), 52601 (2021)
16. Q. Liang, T. Chen, W. H. Bu, Y. H. Zhang, and B. Yan, Laser cooling with adiabatic passage for type-II transitions, *Front. Phys.* 16(3), 32501 (2021)
17. K. Yan, R. Gu, D. Wu, J. Wei, Y. Xia, and J. Yin, Simulation of EOM-based frequency-chirped laser slowing of MgF radicals, *Front. Phys.* 17(4), 42502 (2022)
18. W. Bu, Y. Zhang, Q. Liang, T. Chen, and B. Yan, Saturated absorption spectroscopy of buffer-gas-cooled Barium monofluoride molecules, *Front. Phys.* 17(6), 62502 (2022)
19. Y. Liu and L. Luo, Molecular collisions: From near-cold to ultra-cold, *Front. Phys.* 16(4), 42300 (2021)
20. R. Vicente, G. Nogues, J. M. Niot, T. Wiertz, P. Contini, and A. Gardelein, Impacts of laser cooling for low earth orbit observation satellites: An analysis in terms of size, weight and power, *Cryogenics* 105, 103000 (2020)
21. J. Li, Z. Chen, Y. Liu, P. S. Kollipara, Y. Feng, Z. Zhang, and Y. Zheng, Opto-refrigerative tweezers, *Sci. Adv.* 7(26), eabh1101 (2021)
22. M. P. Hehlen, J. Meng, A. R. Albrecht, E. R. Lee, A. Gragossian, S. P. Love, C. E. Hamilton, R. I. Epstein, and M. Sheik-Bahae, First demonstration of an all-solid-state optical cryocooler, *Light Sci. Appl.* 7(1), 15 (2018)
23. J. Knall, M. Engholm, T. Boilard, M. Bernier, P. B. Vigneron, N. Yu, P. D. Dragic, J. Ballato, and M. J. F. Digonnet, Radiation-balanced silica fiber laser, *Optica* 8(6), 830 (2021)
24. F. Caminati, G. Cittadino, E. Damiano, A. Di Lieto, and M. Tonelli, A design for optical refrigeration: The parallel configuration, *Appl. Phys. Lett.* 122(2), 021102 (2023)
25. P. Pringsheim, Zwei bemerkungen über den unterschied von lumineszenz-und temperaturstrahlung, *Eur. Phys. J. A* 57(11–12), 739 (1929)
26. L. Landau, On the thermodynamics of photoluminescence, *J. Phys. (Moscow)* 10, 503 (1946)
27. W. Patterson, S. Bigotta, M. Sheik-Bahae, D. Parisi, M. Tonelli, and R. Epstein, Anti-Stokes luminescence cooling of Tm^{3+} doped BaY_2F_8, *Opt. Express* 16(3), 1704 (2008)
28. S. Rostami, A. R. Albrecht, A. Volpi, M. P. Hehlen, M. Tonelli, and M. Sheik-Bahae, Tm-doped crystals for mid-IR optical cryocoolers and radiation balanced lasers, *Opt. Lett.* 44(6), 1419 (2019)
29. S. Rostami, A. R. Albrecht, A. Volpi, and M. Sheik-Bahae, Observation of optical refrigeration in a holmium-doped crystal, *Photon. Res.* 7(4), 445 (2019)
30. A. Gragossian, M. Ghasemkhani, J. Meng, A. Albrecht, M. Tonelli, and M. Sheik-Bahae, Optical refrigeration inches toward liquid-nitrogen temperatures, *SPIE Newsroom* (2017)
31. S. Bigotta, A. Di Lieto, A. Toncelli, M. Tonelli, D. Seletskiy, M. Hasselbeck, M. Sheik-Bahae, and R. Epstein, Laser cooling of solids: New results with single fluoride crystals, *Nuovo Cimento-Societa Italiana Di Fisica Sezione B* 122, 685 (2007)
32. B. Zhong, J. Yin, Y. Jia, L. Chen, Y. Hang, and J. Yin, Laser cooling of Yb^{3+}-doped $LuLiF_4$ crystal, *Opt. Lett.* 39(9), 2747 (2014)
33. B. Zhong, Y. Lei, H. Luo, Y. Shi, T. Yang, and J. Yin, Laser cooling of the Yb^{3+}-doped $LuLiF_4$ single crystal for optical refrigeration, *J. Lumin.* 226, 117472 (2020)
34. Y. Lei, B. Zhong, T. Yang, X. Duan, M. Xia, C. Wang, J. Xu, Z. Zhang, J. Ding, and J. Yin, Laser cooling of Yb^{3+}:$LuLiF_4$ crystal below cryogenic temperature to 121 K, *Appl. Phys. Lett.* 120(23), 231101 (2022)
35. J. Zhang, D. Li, R. Chen, and Q. Xiong, Laser cooling of a semiconductor by 40 Kelvin, *Nature* 493(7433), 504 (2013)
36. J. B. Khurgin, Multi-phonon-assisted absorption and emission in semiconductors and its potential for laser refrigeration, *Appl. Phys. Lett.* 104(22), 221115 (2014)
37. S. T. Ha, C. Shen, J. Zhang, and Q. Xiong, Laser cooling of organic–inorganic lead halide perovskites, *Nat. Photonics* 10(2), 115 (2016)
38. X. Xia, A. Pant, A. S. Ganas, F. Jelezko, and P. J. Pauzauskie, Quantum point defects for solid-state laser

refrigeration, *Adv. Mater.* 33(23), 1905406 (2021)
39. J. Zhang, Q. Zhang, X. Wang, L. C. Kwek, and Q. Xiong, Resolved-sideband Raman cooling of an optical phonon in semiconductor materials, *Nat. Photonics* 10(9), 600 (2016)
40. D. Li, J. Zhang, and Q. Xiong, Laser cooling of CdS nanobelts: Thickness matters, *Opt. Express* 21(16), 19302 (2013)
41. S. R. Bowman, Lasers without internal heat generation, *IEEE J. Quantum Electron.* 35(1), 115 (1999)
42. S. R. Bowman, S. P. O'Connor, S. Biswal, N. J. Condon, and A. Rosenberg, Minimizing heat generation in solid-state lasers, *IEEE J. Quantum Electron.* 46(7), 1076 (2010)
43. G. Nemova and R. Kashyap, Thin-disk athermal laser system, *Opt. Commun.* 319, 100 (2014)
44. E. Mobini, M. Peysokhan, B. Abaie, and A. Mafi, Thermal modeling, heat mitigation, and radiative cooling for double-clad fiber amplifiers, *J. Opt. Soc. Am. B* 35(10), 2484 (2018)
45. J. M. Knall, M. Engholm, T. Boilard, M. Bernier, and M. Digonnet, Radiation-balanced silica fiber amplifier, *Phys. Rev. Lett.* 127(1), 013903 (2021)
46. J. M. Knall and M. J. Digonnet, Design of high-power radiation-balanced silica fiber lasers with a doped core and cladding, *J. Lightwave Technol.* 39(8), 2497 (2021)
47. M. Sheik-Bahae and Z. Yang, Optimum operation of radiation-balanced lasers, *IEEE J. Quantum Electron.* 56(1), 1 (2020)
48. G. Nemova and R. Kashyap, Athermal continuous-wave fiber amplifier, *Opt. Commun.* 282(13), 2571 (2009)
49. E. Mobini, S. Rostami, M. Peysokhan, A. Albrecht, and A. Mafi, Laser cooling of ytterbium-doped silica glass, *Commun. Phys.-UK* 3, 1 (2020)
50. E. Mobini, M. Peysokhan, B. Abaie, M. P. Hehlen, and A. Mafi, Spectroscopic investigation of Yb-doped silica glass for solid-state optical refrigeration, *Phys. Rev. Appl.* 11(1), 014066 (2019)
51. M. Peysokhan, E. Mobini, B. Abaie, and A. Mafi, Method for measuring the resonant absorption coefficient of rare-earth-doped optical fibers, *Appl. Opt.* 58(7), 1841 (2019)
52. X. Xia, A. Pant, E. J. Davis, and P. J. Pauzauskie, Design of a radiation-balanced fiber laser via optically active composite cladding materials, *J. Opt. Soc. Am. B* 36(12), 3307 (2019)
53. Z. Yang, J. Meng, A. R. Albrecht, and M. Sheik-Bahae, Radiation-balanced Yb:YAG disk laser, *Opt. Express* 27(2), 1392 (2019)
54. J. B. Khurgin, Radiation-balanced tandem semiconductor/Yb^{3+}: YLF lasers: Feasibility study, *J. Opt. Soc. Am. B* 37(6), 1886 (2020)
55. J. Knall, M. Engholm, J. Ballato, P. D. Dragic, N. Yu, and M. J. Digonnet, Experimental comparison of silica fibers for laser cooling, *Opt. Lett.* 45(14), 4020 (2020)
56. M. Peysokhan, E. Mobini, A. Allahverdi, B. Abaie, and A. Mafi, Characterization of Yb-doped ZBLAN fiber as a platform for radiation-balanced lasers, *Photon. Res.* 8(2), 202 (2020)
57. M. Peysokhan, S. Rostami, E. Mobini, A. R. Albrecht, S. Kuhn, S. Hein, C. Hupel, J. Nold, N. Haarlammert, T. Schreiber, R. Eberhardt, A. Flores, A. Tünnermann, M. Sheik-Bahae, and A. Mafi, Implementation of laser-induced anti-stokes fluorescence power cooling of ytterbium-doped silica glass, *ACS Omega* 6(12), 8376 (2021)
58. R. I. Epstein, J. Brown, B. C. Edwards, and A. Gibbs, Measurements of optical refrigeration in ytterbium-doped crystals, *J. Appl. Phys.* 90(9), 4815 (2001)
59. E. S. L. Filho, G. Nemova, S. Loranger, and R. Kashyap, Laser-induced cooling of a Yb:YAG crystal in air at atmospheric pressure, *Opt. Express* 21(21), 24711 (2013)
60. B. Zhong, Y. Lei, X. Duan, T. Yang, and J. Yin, Optical refrigeration of the Yb^{3+}-doped YAG crystal close to the thermoelectric cooling limit, *Appl. Phys. Lett.* 118(13), 131104 (2021)
61. M. Sheik-Bahae and R. I. Epstein, Optical refrigeration, *Nat. Photonics* 1(12), 693 (2007)
62. D. C. Brown and V. A. Vitali, Yb:YAG kinetics model including saturation and power conservation, *IEEE J. Quantum Electron.* 47(1), 3 (2011)
63. S. D. Melgaard, Cryogenic optical refrigeration: Laser cooling of solids below 123 K, Ph.D Thesis, The University of New Mexico, 2013
64. X. Duan, B. Zhong, Y. Lei, C. Wang, J. Xu, Z. Zhang, J. Ding, and J. Yin, Accurate characterization of the properties of the rare-earth-doped crystal for laser cooling, *Appl. Sci. (Basel)* 12(9), 4447 (2022)
65. H. W. Bruesselbach, D. S. Sumida, R. A. Reeder, and R. W. Byren, Low-heat high-power scaling using InGaAs-diode-pumped Yb:YAG lasers, *IEEE J. Sel. Top. Quantum Electron.* 3(1), 105 (1997)
66. D. McCumber, Einstein relations connecting broadband emission and absorption spectra, *Phys. Rev.* 136(4A), A954 (1964)
67. A. Volpi, Laser cooling of fluoide crystals, Ph. D Thesis, Università di Pisa, 2015
68. G. Nemova and R. Kashyap, Optimization of optical refrigaration in Yb^{3+}:YAG samples, *J. Lumin.* 164, 99 (2015)
69. F. D. Patel, E. C. Honea, J. Speth, S. A. Payne, R. Hutcheson, and R. Equall, Laser demonstration of $Yb_3Al_5O_{12}$/(YbAG) and materials properties of highly doped Yb:YAG, *IEEE J. Quantum Electron.* 37(1), 135 (2001)
70. F. Auzel, F. Bonfigli, S. Gagliari, and G. Baldacchini, The interplay of self-trapping and self-quenching for resonant transitions in solids, role of a cavity, *J. Lumin.* 94–95, 293 (2001)
71. C. Goutaudier, K. Lebbou, Y. Guyot, M. Ito, H. Canibano, A. El Hassouni, L. Laversenne, M. T. Cohen-Adad, and G. Boulon, Advances in fibre crystals: Growth and optimization of spectroscopic properties for Yb^{3+} doped laser crystals, *Ann. Chim.* 28(6), 73 (2003)
72. Y. Nakayama, Y. Harada, and T. Kita, An energy transfer accompanied by phonon absorption in ytterbium-doped yttrium aluminum perovskite for optical refrigeration, *Appl. Phys. Lett.* 117(4), 041104 (2020)
73. D. V. Seletskiy, M. P. Hehlen, R. I. Epstein, and M. Sheik-Bahae, Cryogenic optical refrigeration, *Adv. Opt. Photonics* 4(1), 78 (2012)